Lifetime of nuclear velocity dispersion drops in barred galaxies

Hervé Wozniak and Nicolas Champavert

Centre de Recherche Astronomique de Lyon, 9 avenue Charles André, F-69561 Saint-Genis Laval cedex, France

ABSTRACT

We have made hydro/N-body simulations with and without star formation to shed some light on the conditions under which a central kinematically cold stellar component (characterized by a velocity dispersion drop or σ-drop) could be created in a hot medium (e.g. a bulge) and survive enough time to be observed. We found that the timescale for a σ-drop formation could be short (less than 500 Myr) whereas its lifetime could be long (more than 1 Gyr) provided that the central region is continuously or regularly fed by fresh gas which leads to a continuous star formation activity. Star formation in the central region, even at a low rate as $1\,\mathrm{M_\odot\,yr^{-1}}$, is mandatory to sustain a permanent σ-drop by replacing heated particles by new low-σ ones. We moreover show that as soon as star formation is switched off, the σ-drop begins to disappear.

Key words: Galaxies: active – Galaxies: kinematics and dynamics – Galaxies: nuclei – Galaxies: Seyfert – Galaxies: evolution – Galaxies: spiral

1 INTRODUCTION

The discovery of a sub-kpc central drop in stellar velocity dispersion (σ-drop in short) in three Seyfert galaxies with double bars (Emsellem et al. 2001, hereafter Paper I) has brought this phenomenon to the foreground. In fact, a σ-drop was previously observed in a single object (NGC 6503) by Bottema (1989). To explain the low velocity dispersion in the centre, Bottema & Gerritsen (1997) had to built up a model with a distinct dynamically cold and compact isothermal nucleus in addition to the large scale stellar disc with the same mass-to-light ratio. Others examples can be found in a few papers (Héraudeau & Simien 1998; Héraudeau et al. 1999; Jarvis et al. 1988 for instance) but have been most probably overlooked because of the low signal-to-noise ratio of these observations. More recent observations of larger sample and better signal-to-noise ratio have confirmed (Márquez et al. 2003, Emsellem et al. 2004, Emsellem et al. in preparation) the presence of σ-drop in several single-barred galaxies. However, it is still premature to attempt to make statistics on the frequency of σ-drops in galaxies since a complete and systematic survey is not yet available. More challenging and not yet explained is the observation of σ-drops in elliptical galaxies (e.g. NGC 1404, Graham et al. 1998). The occurrence of σ-drops in such objects should deserve a detailed study.

Wozniak et al. (2003)(hereafter Paper II) found that the stellar σ_{los} drop is the kinematical signature of stars born from a dynamically cold gaseous component. The origin of the drop results from the conspiracy of two factors. First, the new stars are concentrated toward the centre, and since they are just born from the low-dispersion gas component, their dispersion is much lower than for the old stars component. But second, the effect is amplified by the fact that the gas dispersion is also dropping toward the centre (and therefore the new stellar component too). This is due to the strong accumulation of gas toward the centre, in a nuclear disk,

where dissipation is stronger than elsewhere, and where the gas is therefore cooling down efficiently.

The existence of flattened and rapidly rotating nuclear stellar discs has been predicted by Shlosman & Begelman (1989) and further studied by Shlosman et al. (1990). They showed that such stellar discs could remain flattened for a long time since two body relaxation is a slow process.

Thus, a few issues remain opened:

(i) The frequency of σ-drop in galaxies depends on the lifetime of the phenomenon. In Paper II we were not able to give such an estimate. However, even if the frequency of this kinematical effect is still under unknown, it can be firmly stated that it is not a peculiar phenomenon since it is observed in an increasing number of 'normal' galaxies. We give in Table 1 an updated list of σ-drop observations. It is worth noting that σ-drops have been detected using a number of absorption lines from the optical to the near infrared (Mg line triplet at $\lambda\lambda$ 5164, 5173, 5184 Å, CaII triplet at λ 8542 and 8662 Å, ^{12}CO molecular bands at roughly 2.29μm, etc.) which traces various ages of stellar populations. Moreover, σ-drops cannot be data reduction artifacts since stellar kinematics has been retrieved from absorption lines using various techniques.

(ii) Other mechanisms could be at work to remove some kinetic energy from the stellar component. For instance, a massive and concentrated dark halo seems to be able to generate a σ-drop in one of the simulations of Athanassoula & Misiriotis (2002) (their Fig. 13).

(iii) Beyond its intrinsic dynamical lifetime, the detectability of any σ-drop should be also limited by the lifetime of the stellar populations that have been used to trace the kinematics. For instance, in Paper I, σ-drops has been detected using the ^{12}CO bandhead at 2.29 μm.

In this paper, we will specifically address the problem of σ-drop lifetime using a new set of N-body experiments.

Table 1. List of confirmed or suspect σ-drops in the literature.

Object	Morph. Type	Nucleus	Reference	Main abs. lines	Technique
NGC 1068	SA(rs)b	Sy 1/2	Emsellem et al. 2005	Mg b	pPXF[1]
NGC 1097	SB(s)b	Sy 1	Emsellem et al. 2001	^{12}CO 2.3μm	pPXF
NGC 1138	SB0		Simien & Prugniel 2002	Mg b	FFM[2]
NGC 1808	SAB(s:)b	Sy 2	Emsellem et al. 2001	^{12}CO 2.3μm	pPXF
NGC 2639	SA(r)a	Sy 1.9	Marquez et al. 2003	CaII T	CCF
NGC 3021	SAbc		Héraudeau et al. 2003	Mg b	FFM
NGC 3412	SB0(s)		Aguerri et al. 2003	Mg b	FCQ[3]
NGC 3623	SAB(rs)a	Liner	De Zeeuw et al. 2002	Mg b	FCQ
NGC 3627	SBb	Liner/Sy 2	Héraudeau & Simien 1998	Mg b	FFM
NGC 4303	SBbc	Sy 2	Héraudeau & Simien 1998	Mg b	FFM
NGC 4579	SBb	Liner/Sy 1.9	Héraudeau & Simien 1998	Mg b	FFM
NGC 4594	SA(s)a	Sy 1.9	Jarvis & Dubath 1988	Mg b	CCF[4]
NGC 4725	SBab	Sy 2	Héraudeau et al. 1999	Mg b	FFM
NGC 4477	SB0	Sy 2	Jarvis et al. 1988	Fe, Mg b	CCF
NGC 5728	SABb(r)	Sy 2	Emsellem et al. 2001	^{12}CO 2.3μm	pPXF
NGC 6503	SA(s)cd	Liner/HII	Bottema 1989; Bottema & Gerritsen 1997	Fe, Mg b	CCF
NGC 6814	SAB(rs)bc	Sy 1.5	Marquez et al. 2003	CaII T	CCF
NGC 6951	SAB(rs)bc	Sy 2	Marquez et al. 2003	CaII T	CCF
NGC 7177	SBb	Liner/HII	Héraudeau et al. 2003	Mg b	FFM
IC 184	SB(r)a	Sy 2	Marquez et al. 2003	CaII T	CCF
Circinus	SAb	Sy 2	Maiolino et al. 1998	^{12}CO 2.3μm	CCF
NGC 3593†	SA(s)0/a	Sy 2	Bertola et al. 1996	5200–6200Å	FCQ

† edge-on galaxy
[1] Penalized pixel fitting (Cappellari & Emsellem 2004)
[2] Fourier Fitting Method (Franx, Illingworth & Heckman 1989)
[3] Fourier Correlation Quotient (Bender 1990)
[4] Cross-Correlation Function (e.g. Bottema 1989 and reference therein)

2 DESCRIPTION OF THE NUMERICAL EXPERIMENTS

An initial stellar population is set up to reproduce a typical disc galaxy. Positions and velocities for $2.5\,10^6$ particles are drawn from a superposition of two axisymmetric Miyamoto & Nagai (1975) discs of mass respectively M_1 and M_2 (cf. Table 2), of scale lengths respectively 1 and 3.5 kpc and common scale height of 0.5 kpc. Initial velocity dispersions are computed solving numerically the Jeans equations. The initial disc radius is 30 kpc except for run H for which the truncation radius is 50 kpc. The gaseous component of runs A^{sf}, A^{sf}_{400}, A^{sf}_{600} and A^{sf}_{1000} is represented by 50 000 particles for a total mass of $1.1\,10^{10}$ M$_\odot$ distributed in a 6 kpc scalelength Miyamoto-Nagai disc. For the collisionless run A^{nosf} M_1 and M_2 have been proportionally scaled so as to keep the same total mass than A^{sf}.

Evolution is computed with a particle–mesh N-body code which includes stars, gas and recipes to simulate star formation when necessary. The broad outlines of the code are the following: the gravitational forces are computed with a particle–mesh method using a 3D polar grid with $(N_R, N_\phi, N_Z) = (31, 32, 64)$ active cells, the hydrodynamics equations are solved using the SPH technique and the star formation process is based on Toomre's criterion for the radial instability of gaseous discs (cf. Michel–Dansac & Wozniak 2004 for more details). Since we used a log–polar grid, we have improved the pre-computation of self-forces by subdividing each cell in $(n_r, n_\phi, n_z) = (32, 6, 6)$ sub-cells. Self-forces are then linearly interpolated before being subtracted from gravitational forces.

When star formation is active, the radiative cooling of the gas has been computed assuming a solar metallicity. We have also checked that our results are independent of the radial resolution in the central 100 pc by using $N_R = 40$ cells. In Fig. 1 we display the region of the bar for various snapshots. More details on the global evolution of such kind of simulations, with similar initial conditions and star formation on a longer timescale can be found in Michel–Dansac & Wozniak (2004) for instance.

Compared to the simulations used in Paper II, those described in the present paper are much more accurate since we have used 5 times more stellar particles and an improved N−body code. We will only deal with a case extract from a dozen of such simulations of various resolutions and initial setup. However, all our simulations display σ-drops. The generic simulation A^{sf} is thus representative of our database. Another example of simulations with σ-drops are given in Emsellem et al. 2004 for a study of NGC 1068.

Apart from the smaller number of stellar particles ($1.1\,10^6$ particles), the setup of the stellar and gas distribution of run H is similar to others runs. It includes an additional live dark halo made of $2.2\,10^6$ live particles distributed in a Plummer sphere of scalelength 50 kpc and mass $6.46\,10^{11}$ M$_\odot$. As our intention is to check the robustness of our results against the presence of the massive dark halo, a Plummer sphere is a simple but sufficient description of the halo. The setup of initial velocities and velocity dispersions of disc particles is made consistently with the dark matter distribution. Since the interaction between the extended live dark matter spheroid and the stellar/gaseous disc cannot be computed with our particle–mesh code because of the limited vertical range of the grid code, run H has been evolved with GADGET, the tree-based N-body+SPH code developed by Springel, Yoshida & White (2001). We used a adaptive time step based on the dynamical time and limited by the Courant–Friedrichs–Levy condition.

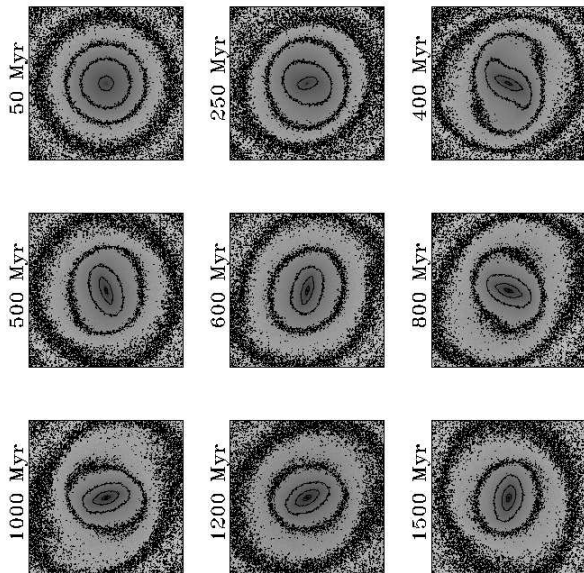H does not exhibit any significant stellar σ-drop up to 5.35 Gyr

Figure 1. Evolution of the central ± 12 kpc of $\mathtt{A^{sf}}$

Table 2. List of runs

Model	Code	End (Myr)	SF stop (Myr)	M_1	M_2	M_g
$\mathtt{A^{nosf}}$	PM	2100	no SF	0.055	0.55	...
$\mathtt{A^{sf}}$	PMSPH	2100	on	0.05	0.5	0.055
$\mathtt{A^{sf}_{400}}$	PMSPH	643	400	"	"	"
$\mathtt{A^{sf}_{600}}$	PMSPH	801	600	"	"	"
$\mathtt{A^{sf}_{1000}}$	PMSPH	1612	1000	"	"	"
H	GADGET	5350	no SF	"	"	"

although others kinematical and morphological stellar properties are roughly similar to halo-dominated models as those described by Athanassoula & Misiriotis (2002) (e.g. flat rotation curve, stellar ring encircling the bar, etc.). The stellar radial velocity dispersion is indeed rather flat, at ≈ 180 km s^{-1} in the central 2 kpc at $t = 5.35$ Gyr. On the contrary, the radial velocity dispersion of the gas drops by 20 km s^{-1} in the central 8 kpc, approximately the diameter of the stellar bar. Others runs, not displayed here, with more massive and/or more extended halos do not develop stellar σ-drops either. Since our star formation recipes have not yet been implemented in GADGET we are not able to check the combined effect of a live dark halo and star formation. The effect of a halo on the σ-drop formation thus deserves a much more in-depth study than the present one. This will be discussed in a future paper.

3 LONG TERM EVOLUTION OF A σ-drop

To estimate the amplitude of a σ-drop (hereafter $\Delta\sigma$), we have chosen to express it as the difference between two representative or mean values of σ: one outside the drop in the kinematically hot part of the bulge ($\sigma_R^{\max}$) and one inside the drop, i.e. the central mean σ ($\sigma_R^{\min}$). Moreover, we will only deal with σ_R for the sake of simplicity since the other two components of the stellar velocity dispersion (σ_θ, σ_Z) also display the same effects (cf. Paper II).
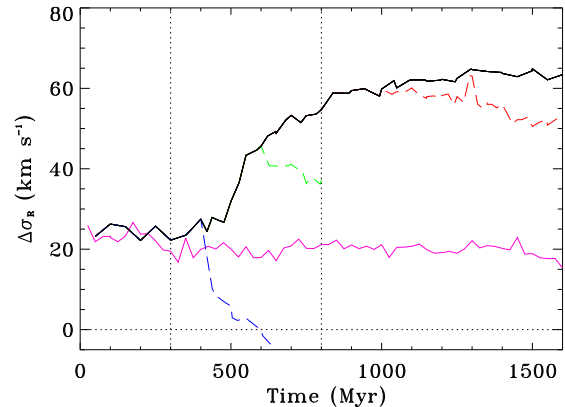

Figure 2. Evolution of the σ-drop amplitude estimated as the difference between σ_R averaged between 450 and 550 pc and the mean σ_R inside the central 200 pc. The reference run $\mathtt{A^{sf}}$ is plotted as a full black line. Star formation has been switched off for runs $\mathtt{A^{sf}_{400}}$ (blue), $\mathtt{A^{sf}_{600}}$ (green) and $\mathtt{A^{sf}_{1000}}$ (red) at, respectively, 400, 600 and 1000 Myr (dashed lines). Vertical dotted lines show where star formation has been switched off. Run $\mathtt{A^{nosf}}$ is also plotted as a full magenta line for reference

Every value of σ_R is obviously a mass-weighted average since new particles may have different mass than initial ones.

To determine the value of $\sigma_R^{\min}$, we have selected a central cylinder of radius 100 pc (i.e. the central 200 pc) at each time. We made several trials with height-limited disc instead of a cylinder but we found no significant differences apart from a higher noise due to lower numbers of particles. The selection typically leads to particle numbers between 4000 and 10000 particles in the central 200 pc.

After some trials, we decided to compute $\sigma_R^{\max}$ in two annuli. The first one, between 450 and 550 pc, represents a 'quiet' region, outside the drop and the close surrounding region, but still in the region that could be considered as the bulge of the galaxy. The second one has been chosen between 250 and 350 pc as being representative of the maximum value of σ_R outside the central drop. The difference between $\sigma_R^{\max}$ in such a region and $\sigma_R^{\min}$ give an extreme value of σ-drop. However, the radius of the maximum σ_R slightly increases during the evolution. We thus found more practical to only use the first annulus (450$-$550 pc) to analyse into some details the typical σ-drop evolution although it slightly underestimates the real $\sigma_R^{\max}$ and thus the real depth of the σ-drop.

$\Delta\sigma$ is displayed in Fig. 2. Its evolution could be roughly separated into three phases. Boundaries of these phases are approximately defined since they should depend on the details of the star formation history in the central region.

3.1 0 $-$ 300 Myr

$\Delta\sigma$ remains approximately constant at 25 km s^{-1}. The comparison with the pure N-body run $\mathtt{A^{nosf}}$ shows that such an amplitude is expected in case of a low star formation rate or no star formation at all. Indeed, it has been shown in Paper II that an artificial σ-drop of such a small amplitude is expected because of N-body softening effects. However, the amplitude of such a numerical σ-drop is much lower than those observed and should fully disappear after convolution by any realistic point spread function.

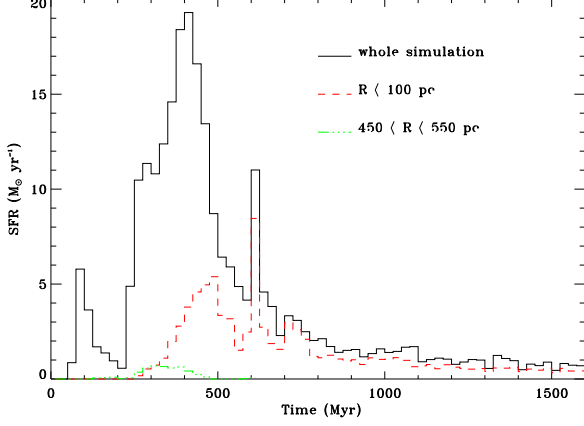The SFR inside the central 200 pc is displayed in Fig. 3. For

Figure 3. Evolution of the star formation rate for run $\mathtt{A^{sf}}$. SFR is displayed for the whole simulation (full line), the central 200 pc (dashed line) and the annulus of radii 450-550 pc (dashed-dotted line)
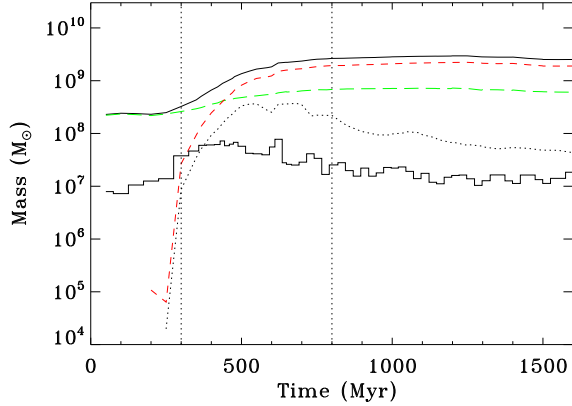

Figure 4. Evolution of the mass inside the central 200 pc for run $\mathtt{A^{sf}}$. The black line is the total mass, the green long-dashed line is the mass of the old population, the red short-dashed line is the mass of the new population, the histogram-like curve is the mass of the gas. The black dotted line is the mass of the new population that is born inside the central 200 pc and is still in this region for the time given in abscissa. Vertical dotted lines show the three phases discussed in the text

$t < 300$ Myr the central SFR remains below 1 $M_\odot$ yr^{-1} while most of the new particles are created in the large scale disc. Thus, at $t = 300$ Myr, the mass of the new population roughly amounts to that of the gaseous component but remains an order of magnitude lower than the old population (cf. Fig. 4).

3.2 $300 - 800$ **Myr**

The σ-drop increase is now very significant so that $\Delta\sigma$ reaches ≈ 55 km s^{-1}. This is the σ-drop growth phase which corresponds to the burst of star formation in the central region. However, such phase could be due either to the decrease of $\sigma_R^{\min}$ or to an increase of $\sigma_R^{\max}$.

To disentangle both effects, we display in Fig. 5 the distribution of σ_R as a function of the epoch of particle formation for several selected times, up to $t = 800$ Myr. The two regions of reference are separately displayed. The old population is included
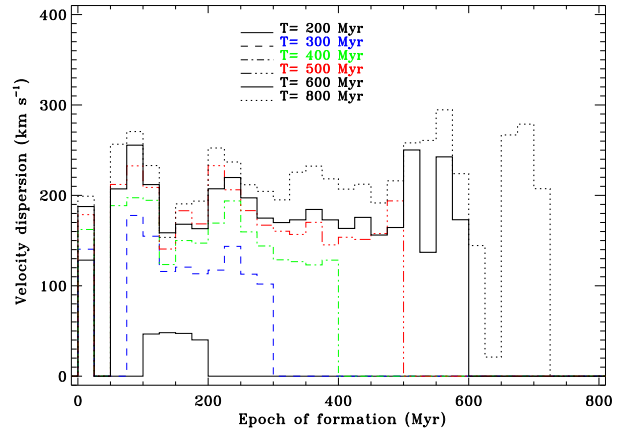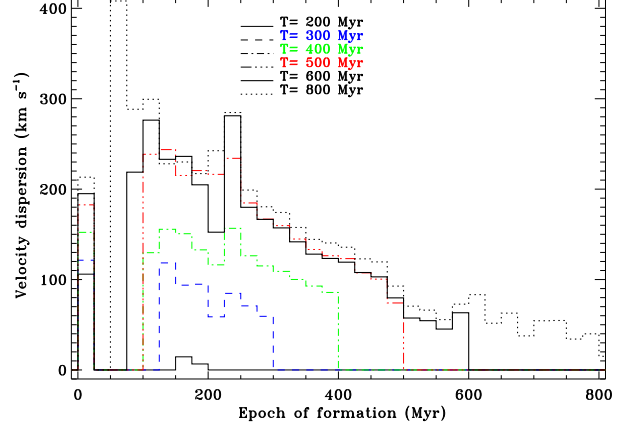

Figure 5. Distribution of σ_R as a function of the epoch of formation for particles selected within a radial range [0, 100] pc (top panel) and [450, 550] pc (bottom panel). Bin size is 25 Myr

in the first bin (0-25 Myr). For each curve, the last bin represents the mean σ_R of the newest particle born during 25 Myr before the corresponding time.

The σ_R distribution in the central 200 pc clearly shows an increase with time between $t = 200$ and $t = 600$ Myr, for all generation of particles. The newest particles have a lower σ_R than the old population as expected. At each time, the shape of the histogram is roughly a linear relationship between σ_R and the epoch of particle formation. In first approximation, the rate of heating is independent of the epoch of formation, i.e. the age of particles. This heating process stops around $t = 600$ Myr. The σ_R distribution then does not evolve any more for particles born between $t = 100$ and $t = 600$ Myr. A number of particles born for $50 < t < 100$ Myr gets into the central region from the outside; these particles have a very high σ_R, greater than the old population, but their total mass is not high enough to increase $\sigma_R^{\min}$.

Another way to represent $\sigma_R^{\min}$ evolution is to display separately the evolution of σ_R for the two particle populations of run $\mathtt{A^{sf}}$ (σ_R^{old} for the initial or 'old' particles and σ_R^{new} for the 'new' particles, i.e. for particles born during the run) and for all the particles (Fig. 6). The control run $\mathtt{A^{nosf}}$ is also plotted to show the heating of collisionless particles for $t \gtrsim 250$ Myr. Such heating is mainly due the development of the stellar bar perturbation which increases the mass in the central region (cf. Paper II). Run $\mathtt{A^{nosf}}$
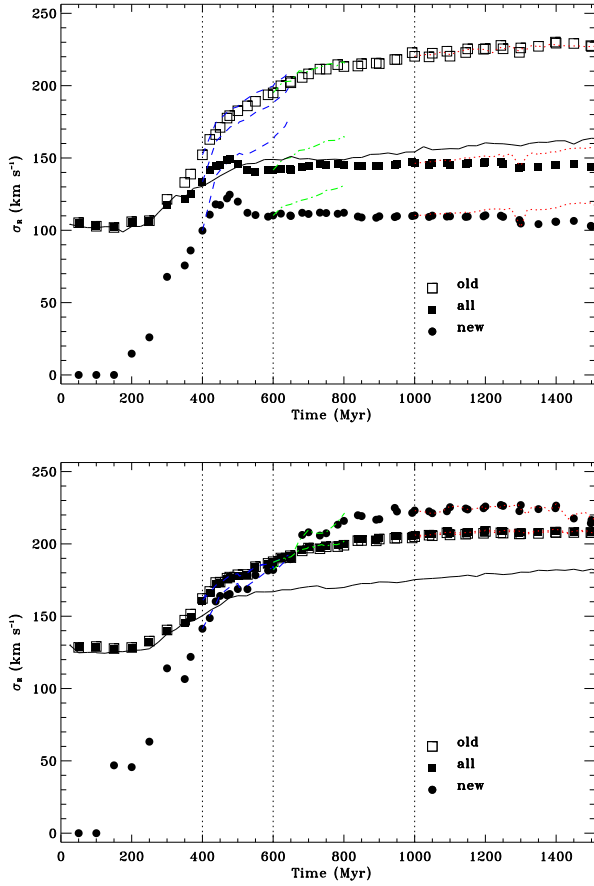
Figure 6. Evolution of σ_R for particles selected within a radial range [0, 100] pc (top panel) and [450, 550] pc (bottom panel). Symbols represent A^{sf}. Opened squares are the velocity dispersion of the initial population (σ_R^{old}), full squares are the total σ_R and full circles are the velocity dispersion of the new particles (σ_R^{new}) created by star formation during the simulation. Runs A_{400}^{sf} (blue dashed lines), A_{600}^{sf} (green dotted-dashed lines) and A_{1000}^{sf} (red dotted lines) can only differ from A^{sf} when star formation is switched off after respectively $t = 400$, $t = 600$ and $t = 1000$ Myr (times are marked by dotted vertical lines). σ_R for the pure N−body run A^{nosf} is plotted as a full line

cannot develop a σ-drop. However, this run allows us to estimate the increase of σ_R due to the secular heating of the central region.

Fig. 6 (top panel) shows that σ_R^{min} clearly increases until $t \approx 475$ Myr and then slightly decreases to reach a plateau around $\sigma_R^{min} \approx 140$ km s^{-1}. The stellar mass in the central 200 pc is mainly made out of new particles, especially for $t \gtrsim 400$ Myr (Fig 4). σ_R^{min} variations are thus strongly correlated to σ_R^{new} ones. The population of new particles responsible for this plateau (those that are born at $600 < t < 800$ Myr) is made out in part of particles born inside the central 200 pc and in part of low σ_R particles that have migrated from the outside. The fraction of new particles which is born and stays in the central region vary from 25 to 10% between $t = 600$ and $t = 800$ Myr. Thus, the migration of low σ_R particles from outside the central 200 pc takes over from particles born inside the central region when the local SFR strongly decreases after $t = 475$ Myr (cf. Fig. 3). This dynamical effect is obviously due to the strong growth of the central total mass which sinks the potential well.

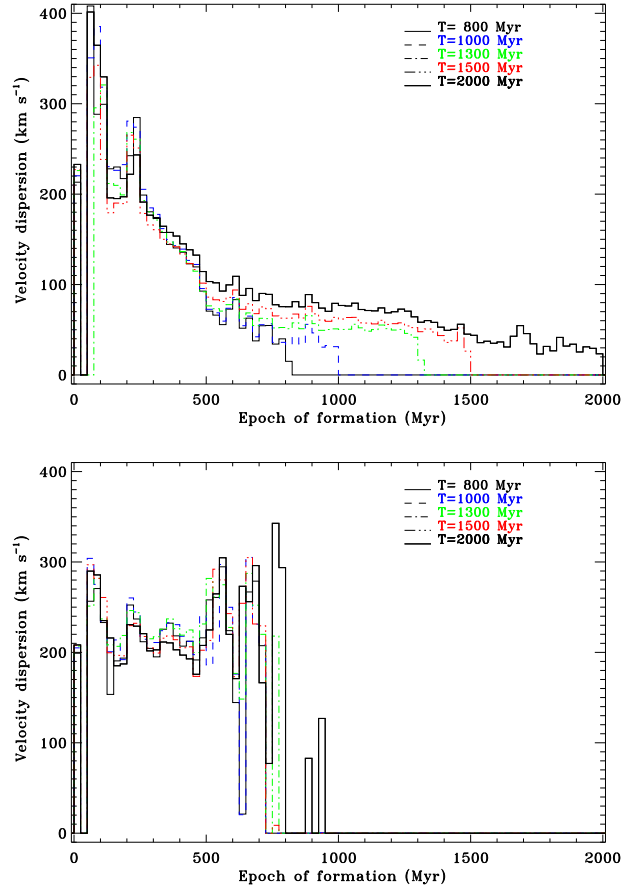The evolution of σ_R^{max} is not driven by the same causes. In-

Figure 7. As Fig. 5 but for $t \geq 800$ Myr. The $t = 800$ Myr curve is the same than for Fig. 5

deed, the σ_R distribution in the 450-550 pc annulus (Fig. 5, bottom panel) does not show any saturation of the heating process. On the contrary to the central region, there is no clear relationship between σ_R and the epoch of formation. This is obviously due to the fact that new particles that are born in the annulus region cannot stay there. Thus, both σ_R^{old} and σ_R^{new} increase. As a consequence, σ_R^{max} continuously grows (Fig. 6, bottom panel), its values being moreover greatly dominated by σ_R^{old} since the old population represents most of the mass in the annulus.

The σ-drop growth is thus due in great part to the heating of the surrounding region, since σ_R^{min} reaches a plateau.

3.3 > 800 **Myr**

During this phase, the σ-drop development seems to saturate. Indeed, $\Delta\sigma$ gains only 10 km s^{-1} in roughly 700 Myr. In the central 200 pc, after $t = 800$ Myr, the slope of the relationship between σ_R and the epoch of formation changes for particles born after $t \approx 500$ Myr (cf. Fig 7). During this phase, the heating is less efficient so that particles born after $t \approx 500$ Myr keep a low σ_R. Moreover, most of the mass in the central region is due to particles born between 250 and 600 Myr, i.e. during the burst of star formation (Fig. 3). Thus, σ_R^{min} does not evolve (cf. Fig 6), as σ_R^{new}, even if σ_R^{old} continues to slightly increase.

The 450-550 pc annulus being dominated by the old population, σ_R^{max} is driven by the behaviour of σ_R^{old} which slightly

increase by a few $\mathrm{km\,s^{-1}}$. It is noteworthy that σ_R^{new} is greater than σ_R^{old} during this phase. This effect is mainly due to particles born between 50 and 625 Myr which cross this region. Finally, since σ_R^{min} does not evolve, the small σ-drop fluctuations are again mainly due to the weak heating of the surrounding region.

For $t > 1300$ Myr, $\Delta\sigma$ fluctuates around a mean value of $65\ \mathrm{km\,s^{-1}}$, with no significant sign of increase or decrease. Thus, a σ-drop is not a transient feature.

4   EFFECT OF SWITCHING STAR FORMATION OFF

To throw some light on the matter of σ-drop lifetime, we have switched off the star formation process at three different times of run $\mathtt{A}^{\mathrm{sf}}$ and pursued the runs (runs are named $\mathtt{A}_{400}^{\mathrm{sf}}$, $\mathtt{A}_{600}^{\mathrm{sf}}$ and $\mathtt{A}_{1000}^{\mathrm{sf}}$) for a while. For $\mathtt{A}_{400}^{\mathrm{sf}}$, star formation has been stopped at $t = 400$ Myr, when the total star formation rate (SFR) is maximum (roughly 20 $\mathrm{M}_\odot\ \mathrm{yr}^{-1}$, cf. Fig. 3). The simulation was then proceeded until $t \approx 650$ Myr. For $\mathtt{A}_{600}^{\mathrm{sf}}$, star formation has been stopped in the middle of the σ-drop growing phase ($t = 600$ Myr) whereas it has been switched off at $t = 1000$ Myr for $\mathtt{A}_{1000}^{\mathrm{sf}}$, when the σ-drop is well developed and closed to be stable.

The first obvious effect of switching off the star formation is the decrease of $\Delta\sigma$ for all the three runs (cf. Fig. 2). For run $\mathtt{A}_{400}^{\mathrm{sf}}$, $\Delta\sigma$ becomes even negative for $t > 600$ Myr which means that the central region becomes hotter than the rest of the galaxy. The heating timescale is very short.

As in Sect. 3, we need to disentangle σ_R variations for both representative regions and thus come back to Fig. 6 where σ_R^{min} and σ_R^{max} of $\mathtt{A}_{400}^{\mathrm{sf}}$, $\mathtt{A}_{600}^{\mathrm{sf}}$ and $\mathtt{A}_{1000}^{\mathrm{sf}}$ are compared to those of $\mathtt{A}^{\mathrm{sf}}$, as well as the contribution of σ_R^{old} and σ_R^{new} to σ_R^{min} and σ_R^{max}.

For $t > 400$ Myr, the mass in the central 200 pc is dominated by the new population when star formation is active, so that σ_R^{min} closely follows σ_R^{new}. Indeed, the mass of the new population continuously increases when star formation is active (Fig. 4) so as to equals the mass of the old population at $t \approx 440$ Myr. Then, the new population dominates the central region. Obviously, this is no more the case when star formation is switched off. Indeed, between $t = 400$ and $t = 600$ Myr, σ_R^{min} of $\mathtt{A}_{400}^{\mathrm{sf}}$ increases by $\approx 55\ \mathrm{km\,s^{-1}}$. The rate at which σ_R^{new} increases is higher ($\approx 0.8\ \mathrm{km\,s^{-1}\,Myr^{-1}}$) during the first ≈ 50 Myr than the following 150 Myr ($\approx 0.1\ \mathrm{km\,s^{-1}\,Myr^{-1}}$, very close to the rate of run $\mathtt{A}^{\mathrm{nosf}}$). A marginal effect is the small heating of the old population ($\approx 10\ \mathrm{km\,s^{-1}}$ at $t = 600$ Myr). The heating of the new population is also very efficient in the 450-550 pc annulus but, since this region is dominated by the old population, the effect on σ_R^{max} is limited to $\approx 25\ \mathrm{km\,s^{-1}}$. Thus the heating of the central region is mainly responsible to the σ-drop disappearance. This heating has mainly two causes:

(i) the rapid gas accumulation in the central region strongly increases the central mass and makes local perturbations of the gravitational potential;

(ii) low-σ particles that escape from the central region are not replaced by new ones. Indeed, the new population is made only in part of particles which are born and remain inside the 200 pc. We show in Fig. 4 how evolves the mass of this sub-population. It clearly decreases which means that a fraction of low-σ particles could be heated outside the central region, during their escape. When star formation is active, they are replaced at each timestep by the last generation of particles. This is no more the case for $\mathtt{A}_{400}^{\mathrm{sf}}$, $\mathtt{A}_{600}^{\mathrm{sf}}$ and $\mathtt{A}_{1000}^{\mathrm{sf}}$.

For $\mathtt{A}_{600}^{\mathrm{sf}}$ and $\mathtt{A}_{1000}^{\mathrm{sf}}$, the decrease of $\Delta\sigma$ has a longer timescale than for $\mathtt{A}_{400}^{\mathrm{sf}}$ even though the same mechanism than for $\mathtt{A}_{400}^{\mathrm{sf}}$ comes into play when the star formation is switched off. The amplitude of the decrease of $\Delta\sigma$ is therefore smaller for $\mathtt{A}_{600}^{\mathrm{sf}}$ than for run $\mathtt{A}_{400}^{\mathrm{sf}}$, and even smaller for $\mathtt{A}_{1000}^{\mathrm{sf}}$. Since the central σ_R^{new} is roughly constant for $600 < t < 1000$ Myr for $\mathtt{A}^{\mathrm{sf}}$ (cf. Fig. 6), one cannot invoke the effect of a colder population which needs more energy to be heated. In fact, the heating of the central region is much more difficult at $t = 600$ or $t = 1000$ Myr essentially because the mass of the new low-σ population is greater than the old one (Fig. 4). Another cause is the bar itself. For $t > 475$ Myr, the gravitational perturbations made by the formation of the stellar bar have vanished. Finally, there is also less gas accumulation in the centre than for $\mathtt{A}_{400}^{\mathrm{sf}}$ since star formation has consumed a significant fraction of the available reservoir in the central region.

5   CONCLUSIONS

We confirm the result found in Paper II that the appearance of a stellar σ-drop in hydro+N$-$body simulations is unavoidable on the condition that star formation is take into account. Indeed, low-σ gas accumulates into a central disc because of the gravitational torques induced by the stellar bar. It gives raise to a new stellar population with the same velocity dispersion. Therefore, the σ-drop appears quickly after the beginning of the bar formation, i.e. ≈ 300 Myr for our simulation $\mathtt{A}^{\mathrm{sf}}$. It takes roughly 1 Gyr to reach the maximum amplitude. Then, the amplitude of the σ-drop remains constant ($\gtrsim 65\ \mathrm{km\,s^{-1}}$) until the end of the simulation (2.1 Gyr). Timescales could however strongly depend on the star formation rate in the central region.

A σ-drop is thus not a transient feature. However, all stellar populations, even low-σ particles, are heated, probably by fluctuations in the central region of the gravitational potential field as those described by, for instance, (Carlberg & Sellwood 1985), or stochastic heating made by resonances between several density waves (Minchev & Quillen 2005). However, in this paper, we did not investigate into details what could be the heating mechanisms since this deserves a dedicated study. The σ-drop persistence is thus not due to some improbable cooling mechanism. Our experiments of switching off the star formation recipes at various epoch prove the relationship between this long lifetime and the refurbishment of the new stellar population of low-σ. A star formation rate as low as $1\ \mathrm{M}_\odot\ \mathrm{yr}^{-1}$ in the central 200 pc is enough to sustain a permanent σ-drop by replacing heated particles by new low-σ ones. Such a rate is not uncommon in barred galaxies provided that the central region is regularly fed by fresh gas. Moreover, when the star formation rate is too low, it will take several hundred Myr for the σ-drop to disappear. This could explain why σ-drops are still observable in early-type galaxies with no sign of nuclear star formation (e.g. NGC 4477).

The visibility of a σ-drop as well as its opposition to heating mechanisms, strongly depends on the mass ratio between the old 'hot' population and the 'new' cold one. For $\mathtt{A}^{\mathrm{sf}}$ the central star formation rate reaches 5 $\mathrm{M}_\odot\ \mathrm{yr}^{-1}$ during the bar formation phase so as to create a new population which becomes more massive than the initial one at $t \approx 440$ Myr, thus on a rather short timescale. σ-drops should thus be rather common in barred galaxies in the local universe. A systematic survey of the central kinematics in barred galaxies could confirm these results.

6 ACKNOWLEDGEMENTS

REFERENCES

Aguerri J.A.L., Debattista V.P., Corsini E.M., 2003, MNRAS 338, 465

Athanassoula E., Misiriotis 2002, MNRAS, 330, 35

Bender, R. 1990, A&A 229, 441

Bertola F., Cinzano P., Corsini E. M., Pizzella A., Persic M., Salucci P., 1996, ApJ 458, L67

Bottema R., 1988, A&A 197, 105

Bottema R., 1989, A&A 221, 236

Bottema R., Gerritsen J. P. E., 1997, MNRAS 290, 585

Carlberg R.G., Sellwood J.A., 1985, ApJ 292, 79

Cappellari, M., & Emsellem, E. 2004, PASP, 116, 138

Emsellem E., Greusard D., Combes F., Friedli D., Leon S., Pécontal E., Wozniak H., 2001 A&A 368, 52 (Paper I)

Emsellem E., Kambiz F., Wozniak H., Ferruit P., Mundell C., Schinnerer E., 2005 MNRAS submitted

Franx M., Illingworth G., Heckman T., 1989, ApJ 344, 613

Graham A.W., Colless M.M., Busarello G., Zaggia S., Longo G., 1998, A&AS 133, 325

Héraudeau P., Simien F., 1998, A&AS 133, 317

Héraudeau P., Simien F., Maubon G., Prugniel P., 1999, A&AS 136, 509

Jarvis B.J., Dubath P., 1988, A&A 201, L33

Jarvis B.J., Dubath P., Martinet L., Bacon R., 1988, A&AS 74, 513

Maiolino R., Krabbe A., Thatte N., Genzel R., 1998, ApJ 493, 650

Márquez I., Masegosa J., Durret F., González Delgado R.M.,Moles M., Maza J., Pérez E., Roth M., 2003, A&A 409, 459

Michel–Dansac L., Wozniak H., 2004 A&A 421, 863

Minchev I., Quillen A.C., 2005, MNRAS submitted (astro-ph/0511037)

Miyamoto M., Nagai R., 1975, PASJ 27, 533

Shlosman I., Begelman M.C., 1989, ApJ 341, 685

Shlosman I., Begelman M.C., Frank J., 1990, Nature 345, 679

Springel V., Yoshida N., White S., 2001, New Astronomy 6, 79

Wozniak H., Combes F., Emsellem E., Friedli D., 2003, A&A 409, 469 (Paper II)